Monthly Notices
of the
ROYAL ASTRONOMICAL SOCIETY

MNRAS **467,** 2301–2314 (2017)
Advance Access publication 2017 February 1

doi:10.1093/mnras/stx254

An instability of feedback-regulated star formation in galactic nuclei

Paul Torrey,[1]★† Philip F. Hopkins,[2] Claude-André Faucher-Giguère,[3] Mark Vogelsberger,[1] Eliot Quataert,[4] Dušan Kereš[5] and Norman Murray[6,7]

[1]*MIT Kavli Institute for Astrophysics and Space Research, Cambridge, MA 02139, USA*
[2]*TAPIR, Mailcode 350-17, California Institute of Technology, Pasadena, CA 91125, USA*
[3]*Department of Physics and Astronomy and CIERA, Northwestern University, 2145 Sheridan Road, Evanston, IL 60208, USA*
[4]*Department of Astronomy and Theoretical Astrophysics Center, University of California Berkeley, Berkeley, CA 94720, USA*
[5]*Department of Physics, University of California at San Diego, 9500 Gilman Drive, La Jolla, CA 92093, USA*
[6]*Canadian Institute for Theoretical Astrophysics, 60 St. George Street, University of Toronto, ON M5S 3H8, Canada*
[7]*Canada Research Chair in Astrophysics*

Accepted 2017 January 26. Received 2017 January 26; in original form 2016 March 23

ABSTRACT

We examine the stability of feedback-regulated star formation (SF) in galactic nuclei and contrast it to SF in extended discs. In galactic nuclei, the orbital time becomes shorter than the time over which feedback from young stars evolves. We argue analytically that traditional feedback-regulated SF equilibrium models break down in the regime. We study this using numerical simulations with the pc-scale resolution and explicit stellar feedback taken from stellar evolution models. The nuclear gas mass, young stellar mass and star formation rate (SFR) within the central ∼100 pc (the short-time-scale regime) never reach steady state, but instead go through dramatic, oscillatory cycles. Stars form until a critical surface density of young stars is present (where feedback overwhelms gravity), at which point they expel gas from the nucleus. Since the dynamical times are shorter than the stellar evolution times, the stars do not die as the gas is expelled, but continue to push, triggering a runaway quenching of SF in the nucleus. However, the expelled gas is largely not unbound from the galaxy, but goes into a galactic fountain that re-fills the nuclear region after the massive stars from the previous burst cycle have died off (∼50-Myr time-scale). On large scales (>1 kpc), the galaxy-scale gas content and SFR is more stable. We examine the consequences of this episodic nuclear SF for the Kennicutt–Schmidt (KS) relation: While a tight KS relation exists on ∼1-kpc scales, the scatter increases dramatically in smaller apertures centred on galactic nuclei.

Key words: stars: formation – galaxies: evolution – galaxies: formation – galaxies: ISM – galaxies: starburst.

1 INTRODUCTION

Observations of star formation (SF) in our Galaxy and in extragalactic systems show that stars are formed inefficiently. A common approach for parameterizing the star formation rate (SFR) efficiency is to express $\dot{\rho}_* = \epsilon \rho_{\rm gas}/t_{\rm ff}$, where $\dot{\rho}_*$ is the SFR per unit volume, $\rho_{\rm gas}$ is the volume density of gas, $t_{\rm ff}$ is the local gas free-fall time and ϵ is the SFR efficiency (i.e. the fraction of gas that turns into stars per galactic free-fall time). Since the volumetric gas and SFR densities are not easily observable, this inefficiency is observationally probed through the Kennicutt–Schmidt (KS; Schmidt 1959; Kennicutt 1998) relation. The KS relation considers the current SFR surface density as a function of the available fuel for SF measured through the total (or molecular) gas surface density. Although there is still debate about the detailed slope and normalization of the KS relation, it is generally agreed that – when measured/averaged over large areas within galaxies – only a few per cent of gas is able to be converted into stars per free fall time (e.g. Zuckerman & Evans 1974; Bigiel et al. 2008; Leroy et al. 2008). Understanding and explaining this inefficiency forms a central component of SF and galaxy formation research.

Two main classes of models have been presented to explain the low efficiency of SF and the form of the KS law. In one class, it is argued that the small-scale properties of supersonic interstellar medium (ISM) turbulence are able to disrupt cloud collapse, giving rise to low SFR efficiencies (e.g. Krumholz & McKee 2005; Federrath & Klessen 2012). These models relate the low efficiency of SF to the statistical properties of the density fluctuations in supersonic

★ E-mail: ptorrey@mit.edu
† Hubble fellow

turbulence. However, since the rate-limiting step for gravitational collapse is the formation of dense gas clouds in the first place, this is an incomplete explanation of the galaxy-scale KS law.

Another approach has been to develop analytic global 'equilibrium' models that explain the low efficiency of SF and form of the KS law (Silk 1997; Thompson, Quataert & Murray 2005; Ostriker, McKee & Leroy 2010; Ostriker & Shetty 2011; Faucher-Giguère, Quataert & Hopkins 2013). The common component of the equilibrium models is that the ISM remains in a quasi-stable state by balancing feedback from young stellar populations with the midplane pressure of the self-gravity of the disc (Silk 1997; Hopkins, Quataert & Murray 2011). While thermal pressure or radiation pressure contribute to the disc support,[1] they play a role in disrupting the giant molecular cloud (GMC) complexes where stars are formed (e.g. Murray, Quataert & Thompson 2010), and could be a source of turbulence; turbulent pressure is thought to provide the dominant source of support against the vertical collapse in gas-rich galaxies (Ostriker & Shetty 2011; Faucher-Giguère et al. 2013), except possibly in the most optically thick inner parts (Thompson et al. 2005). Equilibrium SF models are able to derive SF efficiencies by asserting that the turbulent energy injection rate from young stellar populations balances the turbulent energy dissipation rate. The derived SF efficiencies scale with measurable properties of galactic discs and are broadly consistent with observed SF efficiencies (Ostriker et al. 2010; Ostriker & Shetty 2011; Narayanan et al. 2012; Faucher-Giguère et al. 2013).

These models implicitly assume that (1) gas in the local disc responds to feedback, (2) the strength of feedback scales with the SFR and (3) the SFR – and therefore feedback – responds, in turn, to the gas properties. If feedback is 'too strong,' gas will be expelled or pushed out to such low densities that it cannot form new stars, so the feedback 'supply' will cease. If feedback is 'too weak,' gas collapses rapidly and forms more stars, injecting more feedback until collapse is halted.

This feedback cycle can only hold if the gas adjusts efficiently to the presence of feedback, *and the feedback energy/momentum injection rate efficiently adjusts* to changes in the gas density via the SFR. As long as the feedback is sufficiently strong and efficiently coupled to the gas, the gas will adjust to the presence of feedback. However, there are physical regimes where feedback evolves on time-scales that are (much) longer than the local dynamical time. In these regimes, the feedback energy/momentum injection rate will not respond to changes in the gas density, potentially breaking the feedback loop invoked in these SF models.

For stellar feedback, the primary sources of direct momentum and energy injection into the local environment are photoelectric heating (e.g. Ostriker et al. 2010), radiation pressure, stellar winds, photoionization and SNe (Murray et al. 2010; Hopkins et al. 2011), and cosmic rays (e.g. Jubelgas et al. 2008; Uhlig et al. 2012; Booth et al. 2013; Salem, Bryan & Hummels 2014). Magnetic fields may also act to suppress SF regulation mechanisms (Dolag, Bartelmann & Lesch 1999; Wang & Abel 2009; Pakmor & Springel 2013; Hennebelle & Iffrig 2014; Kim & Ostriker 2015; Marinacci et al. 2015). The relative importance of these mechanisms depends on the physical conditions of the gas.

[1] Thermal pressure typically provides ∼1/4 of the pressure support in atomic-dominated ISM regions, which can be predicted by comparing the thermal pressure yield from photoelectric heating with the turbulent pressure yield from supernovae (SNe; e.g. Ostriker et al. 2010; Kim, Kim & Ostriker 2011; Ostriker & Shetty 2011; Kim, Ostriker & Kim 2013).

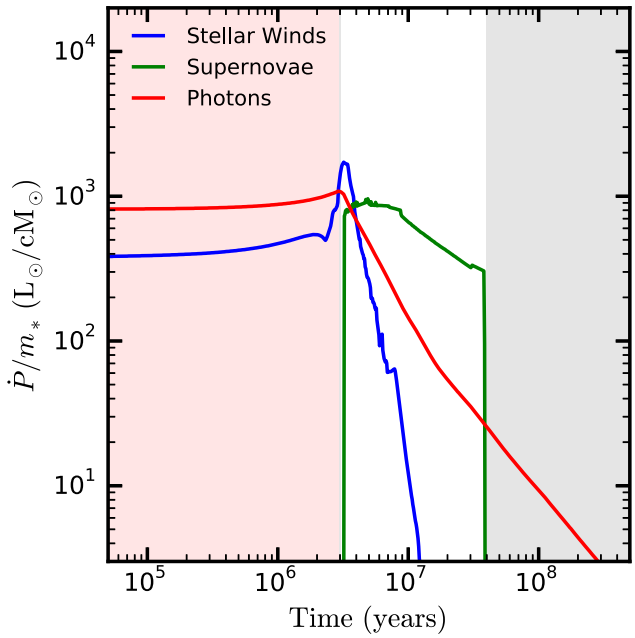

Figure 1. The direct momentum input taken from the STARBURST99 stellar evolution models using a Kroupa IMF. The first ∼3 × 10^6 yr are characterized by nearly constant feedback levels dominated by the radiation pressure from young stars. The direct momentum injections levels begin to evolve only after massive stars begin moving off the main sequence, which leads to a continual decrease in the direct radiation pressure momentum injection and an increase in the supernova momentum injection. We note that the momentum injection values shown are direct momentum injection values and do not account for any gains owing to trapping of photons (i.e. multiple scattering events), gains from pressure confinement of hot gas (the 'b' factor, as defined in equation 11) or losses owing to inefficient coupling. We note that the boost to the direct momentum injection is likely modest for radiation pressure owing to radiation hydro instabilities, but can provide an order of magnitude increase in the supernova contribution to the total momentum injection.

Radiation pressure (Murray et al. 2010) and photoionization (Whitworth 1979; Krumholz, Matzner & McKee 2006; Walch et al. 2012; Sales et al. 2014) are often identified as being responsible for disrupting the dense star-forming gas, but SNe probably dominate the turbulent momentum injection that balances the disc vertical collapse under most conditions (Ostriker & Shetty 2011).

Fig. 1 shows the direct momentum injection budget associated with a single-age stellar population as a function of time since birth taken directly from STARBURST99 (Leitherer et al. 2010). Radiation pressure dominates the early stellar feedback budget until the death of the most massive stars (∼3 Myr) and drops to ∼10 per cent of its initial value by ∼10 Myr. SNe dominate the direct momentum injection budget starting at ∼3 Myr and continue to dominate until the time after which the least massive stars that die in SNe move off the main sequence (∼40 Myr).[2] From Fig. 1, the total momentum injection rate remains nearly constant until ∼3 Myr, and remains variable but order-of-magnitude constant until ∼40 Myr. The constant early momentum injection rates allow us to define an interesting regime: regions of galaxies that possess dynamical times less than the time-scale over which stellar feedback levels adjust. In these regimes, feedback cannot efficiently adjust to changes in the

[2] For a Kroupa initial mas function with $M = 8\,M_\odot$ assumed to be the lower mass limit for SN progenitors.

gas distribution and/or the current SFR. In this paper, we focus on the nuclear regions of galaxies where the small spatial scales and central black hole ensure consistently short dynamical times.

The understanding of SF in galactic nuclei that we present in this paper will set the stage for follow-up studies focused on the accretion, growth and feedback associated with supermassive black holes. Previous studies have considered the impact of stellar and black hole feedback in concert on the central ∼100-pc nuclear disc (e.g. Hopkins et al. 2016). However, those studies lacked the large-scale galactic disc that is important for understanding the long-term behaviour of supermassive black hole accretion and feedback.

The structure of this paper is as follows: In Section 2, we review the basic components of equilibrium feedback models. This allows us to concretely explore the assumptions that break down for the equilibrium model at short dynamical times. We propose alterations to the equilibrium feedback models that hold within short dynamical time regions and conclude that SF within short dynamical time regions is likely to be inherently bursty. In Section 3, we describe the numerical simulations that we use to explore the properties of nuclear SF. In Section 4, we present the results of our numerical simulations, with a focus on the bursty nature of nuclear SF and implications for observations of the KS relation. In Section 5, we present a discussion of our results with implications for observations of nuclear stellar discs as well as the observed KS relation. In Section 6, we summarize and conclude.

2 ANALYTIC ARGUMENTS

2.1 The equilibrium model

Analytic models have been developed to explain the efficiency of SF and form of the KS law. In global equilibrium models, the SF efficiency is derived by asserting that turbulent energy injection from young stellar populations balances the turbulent energy dissipation rate. One of the first models to do this was Thompson et al. (2005), where they examined radiation and mechanical feedback from young stellar populations with a focus on the central 100 pc of a starburst disc. We adopt a similar setup here, which includes an isothermal spherical potential that could represent either a halo or bulge component. The projected surface density follows a power law $\Sigma_{\rm tot} = \sigma^2/\pi G r$. where σ is the velocity dispersion of the potential. The mass profile is given by $M_{\rm tot} = 2\sigma^2 r/G$, with an angular frequency of $\Omega = \sqrt{2}\sigma/r$ set to enforce radial centrifugal balance. The specified gas fraction is $f_{\rm g} = M_{\rm g}/M_{\rm tot} = \Sigma_{\rm g}/\Sigma_{\rm tot}$.

For a thin disc in a spherical gravitational potential, the disc mid-plane pressure as derived from hydrostatic equilibrium is

$$p \approx \phi \rho_{\rm g} h^2 \Omega^2, \tag{1}$$

where h is the disc scaleheight and $\rho_{\rm g}$ is the gas density (see equation 4 in Faucher-Giguère et al. 2013, for further details). The coefficient ϕ is an order of unity constant in the limit of a thin disc in a spherical potential and $\phi \sim 1/Q$ in the limit of a thin disc-dominated potential. This expression for the mid-plane pressure is approximate and requires the assumption of a thin disc, but remains valid for disc- and spheroid-dominated potentials.

Independent of the disc weight calculation, we assume that supersonic turbulent pressure is the primary source of pressure support in the disc. The gas turbulence is described with turbulent gas velocity dispersion $c_{\rm t}$, which gives an effective gas pressure of

$$p \approx \rho_{\rm g} c_{\rm t}^2 \tag{2}$$

and the rate of (volumetric) turbulent energy dissipation of

$$\dot{u} \approx \rho_{\rm g} c_{\rm t}^2 \Omega, \tag{3}$$

assuming $Q \sim 1$ such that $c_{\rm t}/h \sim \Omega$.

Under the assumption that the system approaches an equilibrium, this energy dissipation rate needs to be balanced by feedback from young stars. There are several possible ways to write down the feedback injection rate. Here, we express the energy injection rate from young stars as

$$\dot{u} \approx \frac{p_* c_{\rm t}}{h} = \frac{f_{\rm p} P_*/m_* \dot{\Sigma}_* c_t}{4h}. \tag{4}$$

The second equality follows from expressing the turbulent pressure produced by stellar feedback as

$$p_* = f_p \frac{\rm P_*}{4 m_*} \dot{\Sigma}_*, \tag{5}$$

where P_*/m_* is the radial momentum injected per unit stellar mass formed (Ostriker & Shetty 2011; Faucher-Giguère et al. 2013), and $f_{\rm p}$ parameterizes the efficiency with which the radial momentum drives turbulent energy injection. Numerical simulations have been used to evaluate $f_{\rm p}$ in the molecule-dominated starburst regime (Shetty & Ostriker 2012) as well as the atomic-dominated regime (Kim et al. 2011, 2013), with $f_{\rm p}$ being of the order of unity. Adopting the above expression of the young star pressure/turbulent energy injection rate does not require any assumptions about the origin of the momentum input, and can accommodate multiple momentum input sources (e.g. radiation pressure, SNe, stellar winds, etc.). For SNe, typical values for P_*/m_* are of the order of ∼3000 km s^{-1} (see Ostriker & Shetty 2011, for additional details).

Enforcing balance between the turbulent energy decay and injection rates (i.e. between equations 3 and 4), we find the feedback self-regulated equilibrium condition

$$\rho_{\rm g} c_{\rm t}^2 \Omega \approx \frac{f_{\rm p} P_*/m_* \dot{\Sigma}_* c_{\rm t}}{4\,h}. \tag{6}$$

Using $\Sigma_{\rm g} = 2\,h \rho_{\rm g}$, this can be rearranged in terms of the equilibrium SFR surface density

$$\dot{\Sigma}_* \approx \eta \Sigma_{\rm g} \Omega = \Sigma_{\rm g} \Omega \frac{2 c_{\rm t}}{f_{\rm p} P_*/m_*}, \tag{7}$$

where $\eta = 2c_{\rm t}/f_{\rm p}(P_*/m_*)$ is an efficiency that describes the fraction of gas that can convert into stars in a dynamical time, and where it has been assumed that $Q \sim 1$. This expression shows that the galactic SF efficiency is directly related to the gas turbulent velocity dispersion in the disc.

2.2 Where the equilibrium models break down

The equilibrium model, as described above, breaks down in two regimes.

2.2.1 Equilibrium breakdown from short fynamical times

The equilibrium model breaks down when feedback is unable to modulate its strength on sufficiently short time-scales (i.e. the gas dynamical time-scale). Feedback levels are set by young stellar populations, which evolve based on the rate at which massive stars evolve. Here, we are specifically concerned with the time-scale over which radiation pressure and energy/momentum injection from SNe decline as an initially young stellar population age. Radiation pressure begins to drop when a stellar population is just ∼3-Myr

old, while SN inject significant momentum until ∼40 Myr (Fig. 1). Both of these feedback mechanisms have fallen to a small fraction (∼0.01) of their initial value by the time a stellar population is ∼100-Myr old. In regimes where the dynamical time is much shorter than the stellar evolution time (i.e. $\tau_{\rm SE} \sim 10^6$–10^7 yr; see Fig. 1),[3] feedback will not react sufficiently quickly to changes in the current gas density or SFR, but rather remain strong for a stellar evolution time-scale.

For the one-zone model used in this section, the dynamical time is

$$\tau_{\rm dyn} = \frac{\sqrt{2}\pi r}{\sigma} \sim 10^6\,{\rm yr}\left(\frac{r}{100\,{\rm pc}}\right)\left(\frac{\sigma}{200\,{\rm km\,s^{-1}}}\right)^{-1}. \quad (8)$$

We are using here the orbital time-scale to define the local dynamical time. Other physically relevant time-scales, such as the vertical equilibrium time-scale, could be appropriate for disc equilibrium analysis. However, the orbital and vertical equilibrium time-scales are comparable to up to order of unity constants in our simple analytic framework owing to the assumptions that turbulence is isotropic (i.e. described by a single turbulent velocity), the Toomre Q parameter tends towards unity, and the disc is thin. Comparing this with a stellar evolution time-scale $\tau_{\rm SE}$, we find that the dynamical time will be much shorter than the stellar evolution time ($\tau_{\rm dyn} \ll \tau_{\rm SE}$) when

$$r \ll 1\,{\rm kpc}\left(\frac{\tau_{\rm SE}}{10\,{\rm Myr}}\right)\left(\frac{\sigma}{200\,{\rm km\,s^{-1}}}\right). \quad (9)$$

When this condition is met, massive stars contributing significantly to SNe and radiation pressure live longer than the gas dynamical time and thus feedback from young stars will persist for several dynamical times. For reasonable $\tau_{\rm SE}$ values (e.g. ∼10 Myr), the dynamical time can be much shorter than $\tau_{\rm SE}$ out to a significant fraction of the central 1 kpc. If the feedback from young stars exceeds gravity within this region, then the system becomes unstable/unbound and remains in that state for several dynamical times until the young stars responsible for feedback move off the main sequence.

To explore this regime, we define the convenient quantity $a_*(t) = \dot{P}/m_*$, which has units of acceleration. This quantity is plotted in Fig. 1 as a function of time. We can express the turbulent pressure provided by young stars as

$$p_{*,y} = \Sigma_{*,y} a_*(t) b f_{\rm p}/4, \quad (10)$$

where $\Sigma_{\star,y}$ is the surface density of 'young stars' that dominate the stellar feedback budget. Throughout, we adopt a definition of young stars as being those stars with ages less than 40 Myr. The quantity b accounts for the increase in the momentum provided by stars via trapping of IR photons (Thompson et al. 2005) or by SN acquired during the Sedov–Taylor phase (e.g. Cioffi, McKee & Bertschinger 1988; Gatto et al. 2015; Kim & Ostriker 2015; Martizzi, Faucher-Giguère & Quataert 2015). The total momentum injection per unit stellar mass (P_*/m_*, used in the previous section) is related to $a_*(t)$ via

$$P_*/m_* = \int_0^\infty a_*(t) b\,{\rm d}t, \quad (11)$$

where the boost factor b is folded into the total momentum injection. Setting the turbulent energy injection rate from young stars equal to the turbulent energy dissipation rate given by equation (3), we find the critical surface density of stars

$$\Sigma_{*,y}^{\rm crit} \approx \frac{2\Sigma_{\rm g} c_{\rm t} \Omega}{f_{\rm p} a_*(t) b} = \frac{\pi G \Sigma_{\rm g}^2}{f_{\rm p} a_*(t) b}. \quad (12)$$

This result is similar to the argument in Fall, Krumholz & Matzner (2010) and Murray et al. (2010), when individual star clusters disperse GMCs, but now we apply it to a galaxy nucleus that is allowed to have many independent self-gravitating clouds.

We briefly note that the same critical condition can be derived by considering the pressure – rather than energy – balance. Specifically, equating equations (1) and (5) yields the same critical surface density of young stars. This equivalence is built into the model with the assumption that the disc mid-plane pressure is related directly to the turbulent energy injection and dissipation rates.

Defining the young stellar fraction as

$$f_{*,y} \equiv \frac{\Sigma_{*,y}}{\Sigma_{\rm tot}}, \quad (13)$$

we can write down the critical young stellar fraction or critical young star surface density in terms of the total surface density:

$$f_{*,y}^{\rm crit} \equiv \frac{\Sigma_{*,y}^{\rm crit}}{\Sigma_{\rm tot}} \sim \frac{2 f_{\rm g} c_{\rm t} \Omega}{f_{\rm p} a_*(t) b} \sim \frac{\pi G f_{\rm g} \Sigma_{\rm g}}{f_{\rm p} a_*(t) b}. \quad (14)$$

If we assume a boost factor of $b = 20$ and $a_*(t) = 1000\,{\rm L_\odot\,c^{-1}\,M_\odot}$, this reduces to

$$f_{*,y}^{\rm crit} \approx 1.5 \times 10^{-2} f_{\rm g}\left(\frac{\Sigma_{\rm g}}{10^3\,{\rm M_\odot\,pc^{-2}}}\right). \quad (15)$$

If this critical surface density of young stars is exactly maintained, feedback-driven turbulence and disc self-gravity will be in equilibrium. However, it follows that overshooting this critical young stellar surface density will lead to outflows, which will lower the system's gas fraction, and lead to a runaway outflow condition *that will persist for several local dynamical times*.[4] For this reason, we argue that the critical surface density of young stars is an unstable critical point that will likely lead to a full shut down of star formation with the system going into an outflow state for a stellar evolution feedback time-scale.

After the young stellar populations have aged and their feedback levels have been reduced, gas will return to the nuclear region. Gravitational torquing of gas via asymmetric disc potential features can drive gas mass influx rates of the order of $\dot{M} \sim -|a|^\beta\,\Sigma_{\rm g} R^2 \Omega$, where $|a|$ is the asymmetric disc mode strength and $\beta = 1$–2, depending on whether we are in the linear or non-linear torquing regime (see Hopkins & Quataert 2011, for more details). This can repopulate the central gas reservoir within a few dynamical times, which will allow for a repetition of the central gas blowout cycle.

This result stands in contrast to the 'self-regulating' feedback balance that applies to most of the disc. The key difference is whether or not the feedback-driven turbulent pressure adjusts rapidly or slowly compared to the local dynamical time. Typical galactic dynamical times at ∼kpc distances are of the order of ∼100 Myr (i.e. longer than the time-scale over which stellar feedback evolves). Upward perturbations to the SFR do not lead to a blowout under

[3] In what follows, our analysis does not require that we identify a specific value of $\tau_{\rm SE}$.

[4] We caution that outflows can occur throughout our simulated discs even when this condition is not met. The condition here will result in a strong, nearly complete depletion of the local central gas reservoir, whereas a steady level of gas outflow can be present elsewhere in the disc even when this condition is not met.

normal 'equilibrium' conditions because stars die on time-scales much shorter than the local dynamical time. Where this is the case, there is not enough time for minor SFR perturbations to affect the galaxy dynamics.

2.2.2 *Equilibrium breakdown from insufficient feedback*

Expressing the critical young star surface density as a fraction of the gas mass yields

$$\frac{\Sigma_{*,y}^{\rm crit}}{\Sigma_{\rm g}} = \frac{2c_{\rm t}\Omega}{f_{\rm p}a_*(t)b} = \Omega\frac{Q\sigma\, f_{\rm g}}{\sqrt{2}f_{\rm p}a_*(t)b}. \quad (16)$$

An interesting limit is found by considering when the fraction of gas that must be turned into stars in order to achieve feedback balance is of the order of unity (i.e. $\Sigma_{*,y}^{\rm crit}/\Sigma_{\rm g} \sim 1$). This limit occurs for

$$\Sigma_{\rm g} = \frac{f_{\rm p}a_*(t)b}{\pi QG} \approx 2.7\times10^{11}\frac{{\rm M}_\odot}{{\rm kpc}^2} \quad (17)$$

for $b = 20$ and $a_*(t) = 1000\,{\rm L}_\odot\,c^{-1}\,{\rm M}_\odot$. At this gas surface density, feedback can efficiently oppose gas collapse only by converting an order of unity fraction of the gas mass into stars. This critical surface density value approximately corresponds to the maximum observed stellar surface density in a wide range of dense stellar systems (Hopkins et al. 2010) and represents a feedback failure mode that will be explored in more detail in a forthcoming paper (Grudic et al., in preparation).

3 NUMERICAL METHODS

We investigate the galactic nuclear burst/quench cycles described above using numerical simulations.

3.1 Simulation code

The simulations presented in this paper were performed using the *N*-body hydrodynamics code GIZMO (Hopkins 2015). GIZMO is originally derived from GADGET (Springel 2005) and contains modifications centred around the ability to employ several fundamentally different hydro solvers. In this paper, we employ GIZMO using the meshless-finite-mass method to solve the hydrodynamic equations of motion.

In addition to gravity and hydrodynamics, all simulations include a list of physical processes important to galaxy formation. The specific galaxy formation model used in this paper is the FIRE feedback model (Hopkins et al. 2014). This model has been explored extensively in previous papers simulating the evolution of galaxies within cosmological volumes. The FIRE model is capable of reproducing many observed galaxy properties including the stellar mass–halo mass relation, KS law (Hopkins et al. 2014), the covering fractions of neutral hydrogen in the haloes of $z = 2$–3 Lyman break galaxies (Faucher-Giguère et al. 2015), and can self-consistently generate galactic winds that regulated galaxy mass growth consistent with observational requirements (Muratov et al. 2015).

Details of the FIRE feedback model are given in Hopkins et al. (2014), which we summarize briefly here. All simulations include radiative gas cooling and star formation with associated feedback. Supermassive black hole particles are included in the present simulations because their gravity is dynamically important. However, no black hole feedback is included. Gas cools radiatively under the assumption of local thermodynamic equilibrium down to 10 K. Dense/cold gas clouds are allowed to form stars if they are locally self-gravitating. The SFR is given by $\dot{\rho}_* = \rho_{\rm mol}/t_{\rm ff}$, where the molecular fraction, $f_{\rm H_2}$, is inferred as a function of local gas column density and metallicity following Krumholz & Gnedin (2011). Newly formed stars provide feedback to the ISM through thermal heating via SNe, photoionization, local and long-range radiation pressure, and stellar winds. Each of these feedback sources has a well-defined fiducial level that is adopted directly from STARBURST99, given a stellar particle's age and metallicity (Leitherer et al. 2010).

Table 1. The properties of the initial conditions used for the three isolated discs presented in this paper. Below, $M_{\rm tot}$ is the total mass of each system and $m_{\rm p}$ is the baryon particle mass. Adaptive gravitational softening lengths are employed with ϵ being the minimum (Plummer equivalent) force-softening length used for each particle type.

ID		Gas disc	Halo	Stellar disc
D1	$M_{\rm tot}$ ($M_\odot$)	1.11×10^9	1.32×10^{11}	4.45×10^9
	$m_{\rm p}$ ($M_\odot$)	10^3	8.0×10^4	3.0×10^3
	ϵ (pc)	1	10	2
D2	$M_{\rm tot}$ ($M_\odot$)	2.72×10^9	3.23×10^{11}	1.09×10^{10}
	$m_{\rm p}$ ($M_\odot$)	10^3	8.0×10^4	3.0×10^3
	ϵ (pc)	1	10	2
D3	$M_{\rm tot}$ ($M_\odot$)	1.11×10^{10}	1.32×10^{12}	4.45×10^{10}
	$m_{\rm p}$ ($M_\odot$)	10^3	8.0×10^4	3.0×10^3
	ϵ (*pc*)	1	10	2

3.2 Initial conditions

We employ initial conditions that are modelled after redshift $z = 0$ isolated star-forming late-type galaxies. The initial distribution of particles is sampled based on the scaling relations of Mo, Mao & White (1998) via the procedure outlined in Springel & White (1999). We construct three isolated galaxies that are similar in their physical characteristics but varied in initial mass to use as initial conditions.

The three galaxies have total masses of $M_{\rm tot} = \{1.39\times10^{11}, 3.37\times10^{11}, 1.39\times10^{12}\}\,{\rm M}_\odot$. Each of these galaxies consists of a dark matter halo, stellar disc, stellar bulge, gaseous disc (with 20 per cent gas fraction) and central supermassive black hole. The three systems are similar as they all contain 4 per cent of their mass in the disc, a constant (small) fraction in the central supermassive black hole, 1 per cent of their mass in the bulge, and the rest of the mass in the halo (see Table 1). The stellar and gaseous discs are given exponential surface density profiles with the same disc scale-length set by the halo spin parameter of $\lambda = 0.04$ ($R_{\rm d} = \{1.7, 2.3, 3.7\}$ kpc). The relative masses in stars and gas is set by the initial disc gas fraction, for which we adopt 20 per cent. The discs are initialized to be nearly in equilibrium (e.g. with $Q \sim 1$). The dark matter halo and stellar bulge are set up using a Hernquist (1990) profile initial density distribution. An NFW (Navarro, Frenk & White 1997) equivalent concentration parameter of $C = 10$ is used for all systems. The bulge scale-length is set to be 0.2 times the stellar and gaseous disc scale-lengths. The single supermassive black hole is included in each galaxy as a collisionless particle that is initially placed at the centre of each galaxy. Since the mass of the supermassive black hole is much larger than the typical gas or stellar particle mass, it remains close to the potential minimum of the host galaxy via self-consistently captured dynamical friction without any additional special treatment. Additional values such as the force softening, mass resolution and

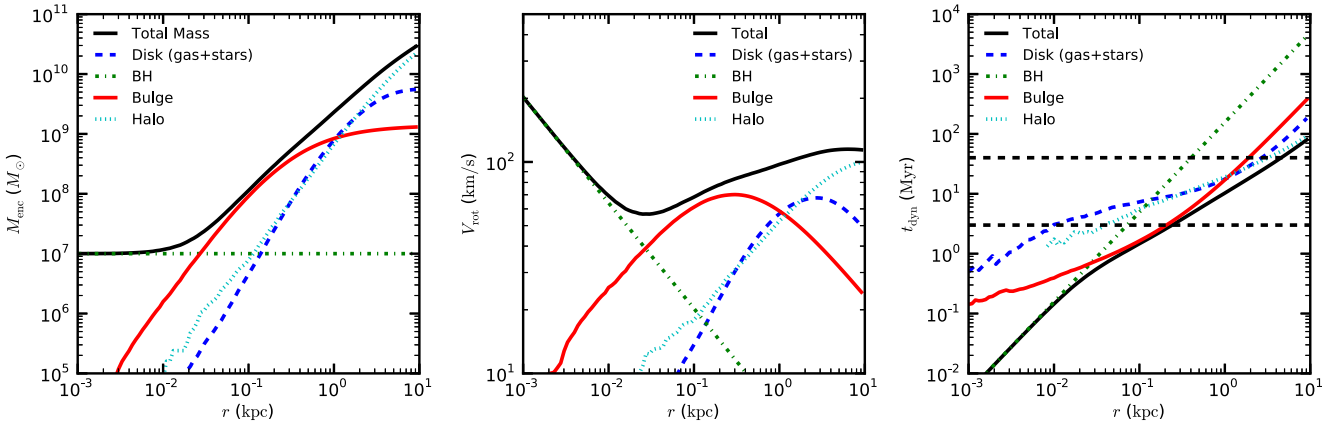

Figure 2. The mass enclosed (left-hand panel), rotational velocity (centre panel) and dynamical time (right-hand panel) are shown as a function of radius for the D1 (low-mass) initial disc. The black hole's dynamical relevance at scales $r \lesssim$ 10–30 pc can be identified from any of the plots. The horizontal lines in the dynamical time plot indicate 3 and 40 Myr. Dynamical times are calculated using the enclosed mass profiles to determine the circular velocities.

naming convention that we used for this initial condition set are summarized in Table 1.

The initial gas distribution does not contain significant manually imposed turbulence, and only modest initial thermal pressure support. A small number (=30) of minor density perturbations (factor of <2 density contrast) and velocity perturbations ($\sim$ 10 km s^{-1}) are imposed at randomly selected places within the disc to prevent a pathologically smooth initial gas disc collapse. These perturbations seed locations where some of the first simulation star particles form. Once SF begins, and feedback follows, the turbulence builds up in the discs self-consistently. There is therefore a brief relaxation time at the beginning of the simulation. We have tested several minor variations of the initial conditions presented in this paper (including Initial Conditions without any density perturbations, or with varied number of induced initial perturbations) and found that while the relaxation time can be significantly extended, the late-time evolution is qualitatively unmodified.

Fig. 2 shows the mass profiles, rotational velocity curves and radially dependent dynamical time for our fiducial low-mass galaxy (D1). The dynamical times are defined using the enclosed mass profiles to calculate the circular velocity. Although we neglect black hole accretion and feedback in these sets of simulations, the presence of this massive particle is important owing to its impact on the dynamics of the nuclear region. The presence of the central supermassive black hole dominates the mass enclosed and rotation curve for the inner 10–30 pc. The rotational velocity curves have a non-monotonic profile, but the dynamical time continually drops towards the galaxy centre. The characteristic stellar evolution timescales of $\sim$3 and $\sim$40 Myr are identified with horizontal dashed lines in the right-hand panel of Fig. 2. We identify 3- and 40-Myr lines because this roughly corresponds to the time when stars begin moving off the main sequence and when the most of the energy from the newly formed stellar population has been deposited, respectively. For this setup, the dynamical time drops below $\sim$3 Myr at a radius of $\sim$100 pc, which changes only slightly for the other initial discs. Within this region, we expect SF and gas supply to be unable to achieve a steady-state solution owing to the short dynamical times. The presence of a 10^7 M$_\odot$ black hole alone keeps the dynamical time below 3 Myr for the central $\sim$100 pc, but a massive/compact stellar bulge could play a similar role in shaping the inner galactic potential.

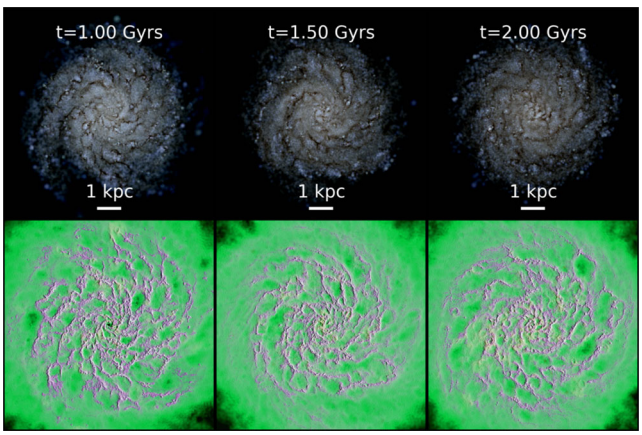

Figure 3. The projected gas surface density is shown at three snapshots during the evolution of the D1 system. The top row shows synthetic SDSS-*g*-, *-r*-, *-i*-band images made using a simple line-of-sight attenuation model. The bottom row shows the gas surface density, with magenta indicating atomic/molecular gas ($10 < T < 8 \times 10^3$ K), green indicating warm ionized gas ($8 \times 10^3 < T < 8 \times 10^5$ K), and yellow (though little is present) hot gas ($T > 10^5$ K). The time of each snapshot is marked in the top row and the scale bar of 1 kpc is also indicated. From the initially smooth gas distribution, a turbulent ISM develops, with dense star-forming regions being continually formed by self-gravity and destroyed through feedback from young stars.

4 RESULTS

4.1 Gas distribution and galaxy structure

Fig. 3 shows a time sequence of the D1 galaxy evolved from 1 to 2 Gyr. The top panel shows a synthetic optical image of the galaxy, while the bottom panel shows the gas content. As indicated in both panels, throughout the entire simulation, the disc remains globally stable without any strong bars developing (although there is a prominent spiral pattern). This global stability is by construction. As the simulation proceeds, gas cools and collects into dense star-forming clumps that are embedded in a volume-filling warm phase of the ISM. The colour of the gas distribution on the bottom panel highlights this multiphase structure: Magenta gas indicates atomic/molecular material, while green indicates warm ionized gas. These star-forming clumps are eventually disrupted through

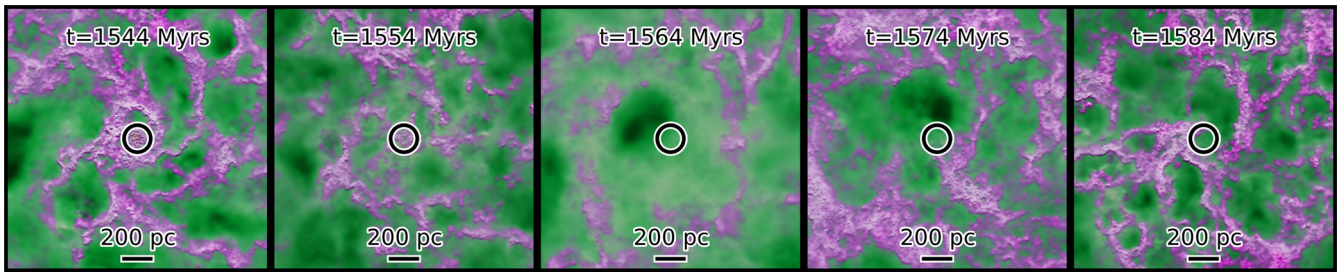

Figure 4. The projected gas surface density is shown at five snapshots during the evolution of the D1 system, focused around the galactic nucleus during a period of nuclear gas blowout. The white circle indicates a cylindrical aperture of 100 pc centred on the central supermassive black hole, which stays closely pinned to the potential minimum. Significant molecular gas is initially present in the central 100-pc aperture. The concentration of cold/molecular gas (indicated with purple) in the nuclear region in the first (leftmost panel) snapshot has an associated elevated level of nuclear SF. Soon after, the feedback from young stars hits the critical level, leading to a near complete blowout of gas within the central 100 pc. The gas density remains suppressed for the next ∼30 Myr, while the feedback from young stars continues to be efficient in spite of the absence of much ongoing SF.

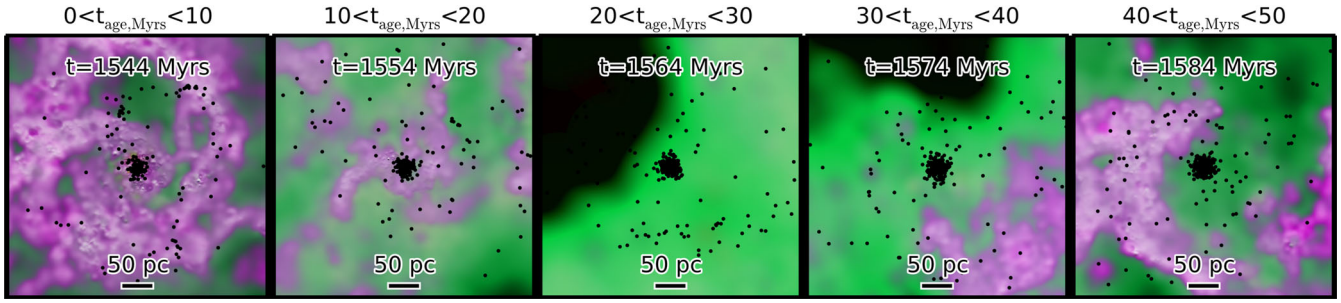

Figure 5. Same as Fig. 4, but zoomed further on the galaxy nucleus and with the locations of young star particles identified with black circles. The left-hand panel indicates the locations of the youngest stars that are highly clustered and generally coincide with the dense gas in which they were formed. Subsequent panels show the same star particles as they age. By a few tens of millions of years, the distribution of young stars becomes more randomized in this region with the stellar populations being well separated from their birth clouds. This is partially driven by feedback, but aided significantly by the short dynamical times on these scales.

feedback from young stars. The self-regulation of a multiphase ISM through feedback from stars using the FIRE feedback model has been discussed extensively in Hopkins et al. (2014). Although we show results here for only the D1 disc, we note that D2, and D3 show qualitatively indistinguishable behaviour.

The multiphase ISM stretches across the full radial range of each galaxy, including the central region. To highlight the evolution of the ISM phase structure in the nuclear region, Fig. 4 shows the gas surface density within a narrow field of view focused on the galactic nucleus at several times. We can identify here the ISM structure extending down to $\lesssim$100-pc scales. The gas density in the central region can be seen to fluctuate through the images. The most severe gas fluctuations are short-lived, and so we have selected times that highlight a period of central gas blowout. The typical blowout cycle begins with a concentration of molecular (purple) star-forming gas in the central ∼100 pc, as is found in the leftmost panel. This dense gas concentration forms stars rapidly until the feedback from these young stars reaches the critical $f_{*,y}^{\rm crit}$ value. This transition occurs very rapidly as the dynamical times on these scales is only ∼1 Myr (see Fig. 2). After gas is removed from the central region, the gas remains at very low densities for ∼20–30 Myr (i.e. the third and fourth panels). By ∼50 Myr (the rightmost panel), molecular gas begins to build up again just outside of the central region. Asymmetric disc features are clearly present, which foster the torquing of gas to the central 100 pc.

In addition to considering the gas distribution on these scales, we consider the distribution of young star clusters and their evolution with time. Fig. 5 shows the evolution of the stellar populations associated with this same blowout event. Specifically, the stellar population that was less than 10-Myr old is identified in the leftmost panel, and those same particles are tracked forward in time. In the leftmost panel, the young stars (here $t < 10$ Myr) take on a clustered distribution that is (mostly) coincident with the dense star-forming gas. In some cases, young stars are found in low-density regions when they have already been able to blow apart their birth cloud. Within 10 Myr (second panel from left), the stars have already randomized their locations significantly. There is little correlation between these young stars and the dense gas distribution. By 20 Myr (central panel), the stars continue to deposit significant momentum and energy via SNe but the gas is almost completely evacuated. However, once the feedback from this young stellar population recedes (two rightmost panels), dense/cold molecular gas quickly returns to the central region.

From Fig. 5, we identify that SF occurs in several distinct self-bound dense gas clouds within the central ∼100 pc. However, the young stars rapidly decouple from their birth clouds owing to both feedback and the short dynamical time. The rapid mixing of the young stellar populations drives the whole central region to react homogeneously to the presence of strong feedback. Despite the presence of multiple self-bound star-forming clumps, the feedback response of the gas in the whole nuclear region acts like that of a single molecular cloud: Stars form until a critical surface density of young stars is present (such that feedback overwhelms gravity) at which point they begin to expel gas from the nuclei.

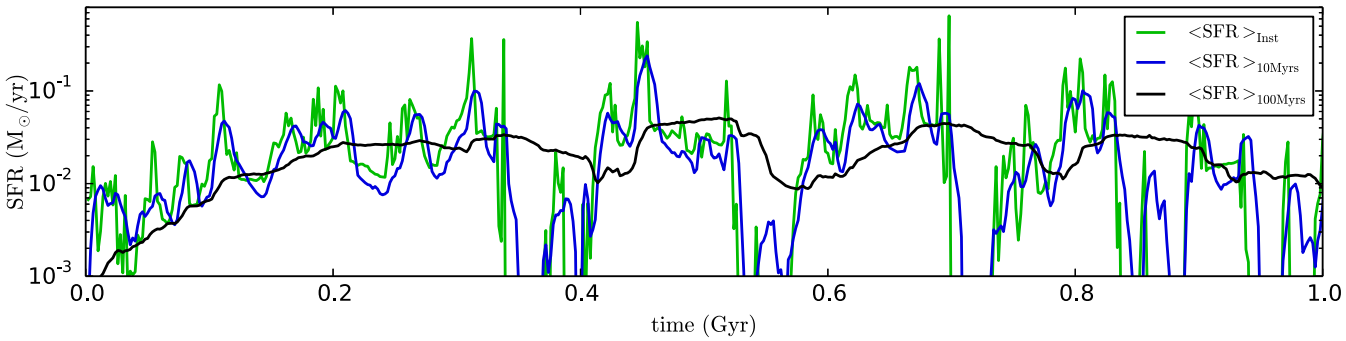

Figure 6. The SFR within the central 100 pc as a function of time for the D1 disc using the instantaneous SFR (green line), the mass of stars formed over the past 10 Myr (blue line) and the mass of stars formed over the past 100 Myr (black line). The mass of young stars gives a smoothed estimate of the SFR and provides a better match to observational SFR probes. We exclusively use the mass of young stars formed in the past 10 Myr (blue line) to determine the SFR throughout the rest of this paper.

4.2 SFRs and gas masses over time

Fig. 6 shows the SFR within the central 100 pc for the D1 galaxy. We show the SFR when taken as an instantaneous value from the simulation, as well as averaged over the past 10 and 100 Myr by calculating SFR $= M_*(t < t_0)/t_0$, where t is the age of the star and t_0 is the averaging time-scale. We present smoothed definitions of the SFR for two reasons. First, the instantaneous SFR values obtained from the simulations rapidly vary and with significant magnitude. Smoothing the SFRs reduces the very high frequency noise allowing for more clear identification of the mean evolutionary trends. Secondly, observational SFR indicators are not sensitive to the instantaneous SFR, but rather to the total mass of young stars formed over some recent time window. The smoothed definition of the SFR is therefore more in line with what is measured observationally through UV or nebular emission-line SFR tracers (e.g. see table 1 of Kennicutt & Evans 2012). In the rest of this paper, we adopt a definition for the SFR as the average SFR over the past 10 Myr – which would be most similar to what would be measured though Hα SFR measurements.

The SFRs shown in Fig. 6 contain short-period variability (of the order of $\sim$10 Myr) and longer period burst/quench cycles (of the order of $\sim$100 Myr). In our simulations, stars form almost exclusively in very dense gas clumps that are subsequently destroyed by stellar feedback. As such, any sampling of the SFR depends on the sampling of the GMC population. The short-period variability seen in these small aperture SFRs is driven by the formation and destruction of individual GMCs. The longer period burst/quench cycles seen in Fig. 6 represent the oscillations induced by the lack of a stable SF equilibrium owing to the short local dynamical times relative to the stellar evolution time-scale (the main effect studied in this paper).

The episodic central SF activity is directly examined in Fig. 7 for the simulated systems. The panels of Fig. 7 show the time evolution of the gas mass, young stellar mass (i.e. $M_*(t < 40$ Myr)), SFR and critical feedback value from top to bottom. Fig. 7 shows these quantities within the central 100 pc, while 2. 8 shows the same quantities within the central 1 kpc.

Over very long periods of time (i.e. $\sim$1-Gyr time-scales), we find that the central region's gas mass and SFR is characterized by a relatively steady state. The time-averaged SFR or central gas mass evolves only marginally over the full time period shown in Fig. 7. This steady behavior is impressive, given that in the nuclear regions of the galaxies explored here, are being evolved for hundreds of dynamical times. The steady nature of the SFR over $\sim$1-Gyr time-scales is consistent with SF being effectively regulated by stellar feedback. Presumably, however, this would break down on time-scales much greater than $\sim$1 Gyr, where the absence of IGM accretion would lead to disc gas depletion.

On shorter time-scales, the central 100-pc region is characterized by an oscillatory gas mass, SFR and young stellar mass within the nuclear region. The behaviour of each of these components is offset in time but closely related. The central gas mass increases in the absence of current strong stellar feedback until SF becomes efficient in the central region owing to the presence of sufficiently dense, self-bound gas clumps. SF then proceeds efficiently until stellar feedback is sufficiently strong, as defined by equation (12), to balance gas collapse. Once feedback is sufficiently strong, the gas supply is rapidly expelled (characterized by very sharp drops in the central gas content for any of the discs). The young stars that are responsible for the strong feedback continue to inject strong feedback into the nuclear region for $\sim$30–40 Myr causing the gas recovery in this region to be relatively slow. The episodic sharp drops in the central gas content are correlated with the periods of peak young stellar mass. The time-scale for this behaviour is of the order of $\sim$100 Myr – though the detailed duty cycle for this process is not very regular, and is different for our three disc models. The time evolution shown in Fig. 7 can be compared back against the central gas surface density plots shown in Fig. 4. Both figures present a complementary picture of the cyclical gas blowout from the central region.

The behaviour of the same quantities averaged on larger spatial scales becomes significantly more stable. Examining Fig. 8, we find that averaged over the central 1 kpc, the mass of gas and young stars in the central regions shows no clear oscillatory behaviour. The instantaneous SFR (not shown) shows significant variability, which becomes nearly smooth when averaged over 10-Myr periods (the plotted curves). The lower variability on 1 kpc scales is partially driven by averaging over a larger number of individual star-forming GMCs. At any time, several dense gas regions are being sampled. Each of these star-forming gas clouds will be individually disrupted via stellar feedback. However, while feedback operating within the central 100 pc is spatially homogenized owing to the short orbital time-scales, GMC disruption that occurs in longer dynamical time regions only disrupts gas clouds locally and fails to collectively clear material from the region. The lower variability on 1-kpc scales is consistent with the analytic arguments outlined in Section 2 where the orbital time becomes long compared to the stellar evolution time-scale. The rate of gas consumption via SF and gas expulsion

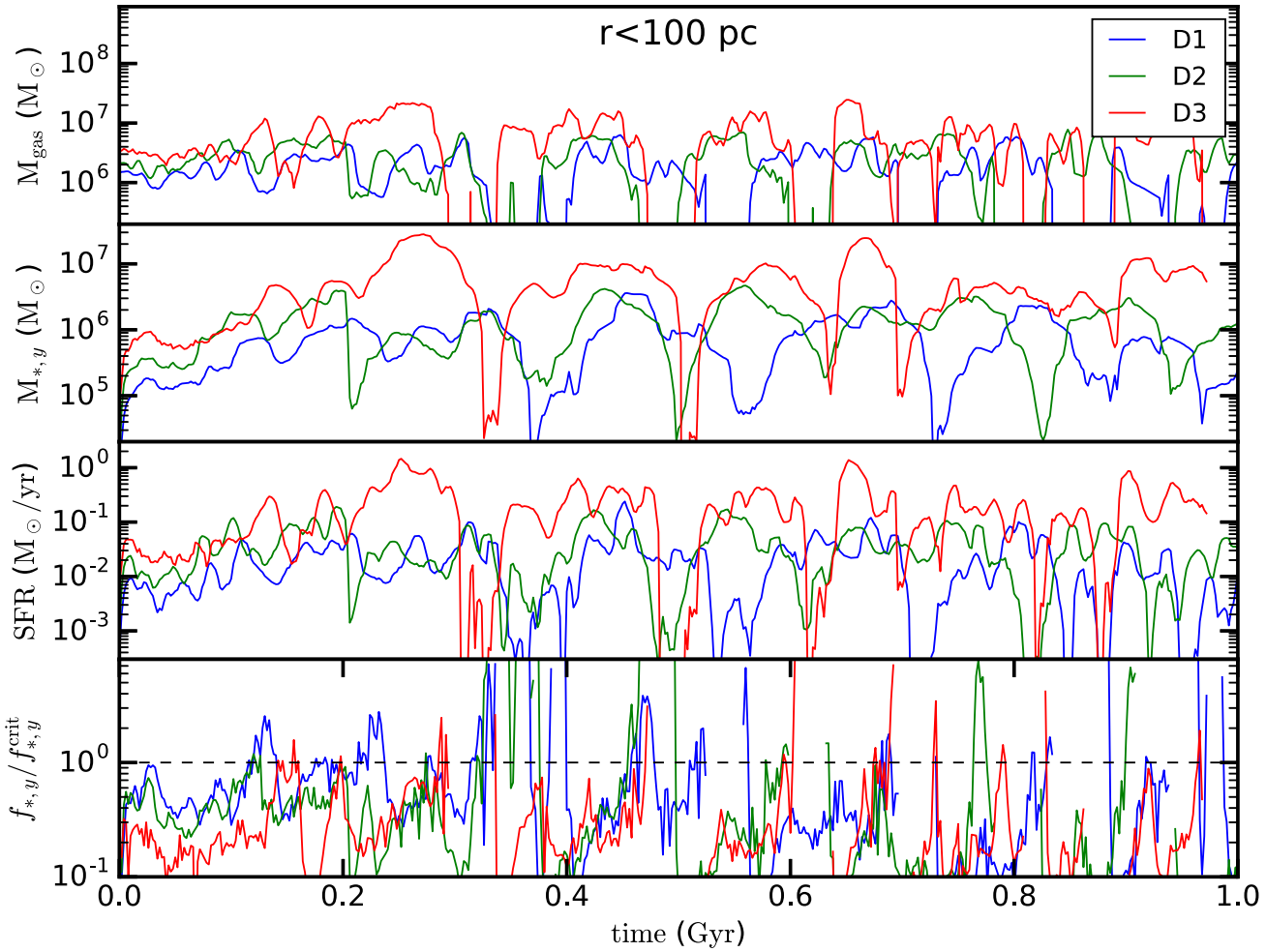

Figure 7. Top to bottom panel: the gas mass, young stellar mass, SFRs and critical young stellar fraction as a function of time for the central 100 pc. The episodic SF in the central 100 pc is clear. Gas content first builds up in the central region, then SF rapidly builds a population of young stars, which drive sufficiently strong feedback to drive down the central gas density.

via feedback are well balanced with the rate of gas return from aging stellar populations and influx from larger radii producing stable gas mass evolution.

The specific spatial scale where we expect feedback-regulated quantities to transition to a stable evolution depends on the assumed time-scale that governs SF based on a few important assumptions that should be treated with caution. In our analysis, we have used the orbital time-scale, but we could have alternatively considered the vertical collapse time-scale. The orbital time-scale is comparable to the vertical collapse time-scale up to the order of unity constants in our model, where we assume that (i) turbulence is isotropic, (ii) $Q \rightarrow 1$, and (iii) the disc is thin. However, these three assumptions do not simultaneously hold in the gas-dominated regime where $c_t \sim \sigma$, and therefore $h/r \sim 1$ (violating the thin disc assumption). Thus, the exact transition radius for stable behaviour may vary in detail in a thick disc, gas-rich model.

Alternatively, we could have adopted, for example, the gas replenishment time-scale over which gas migrates in the galactic nucleus. The central gas replenishment time-scale via gravitational torquing of gas scales as $\tau_{\rm inflow} \sim 1/|a|^\beta \Omega \propto \tau_{\rm dyn}\,|a|^\beta$ (Hopkins & Quataert 2011). For moderate-strength axisymmetric disc, modes this time-scale is a few times larger than the orbital time-scale, which could increase the specific transition radius from stable to unstable feedback-regulated quantities. This would not strongly impact our qualitative conclusions, since our model is primarily intended to distinguish between regions of very large and very small dynamical times with respect to the stellar feedback time.

4.3 The threshold for burst/quench cycles

In Section 2, we derived the surface density of young stars that were required to drive the outflows. The surface density of young stars normalized by the critical surface density, which is expressed in equation (12), is plotted as a function of time in the bottom panels of Figs 7 and 8 for our three discs as evaluated within the central 100 pc and 1 kpc, respectively. Periods of time with $f^{\rm crit}_{*,y} < 1$ indicate that the system has low levels of feedback compared to what is required for gas blowout and is therefore stable/collapsing, while periods of time with $f^{\rm crit}_{*,y} > 1$ indicate that the system is feedback-dominated and is likely driving outflows. The central portion of each galaxy spends the majority of its time in a stable/collapsing state, bookended with brief periods of strong feedback. We can compare the periods of time with high $f^{\rm crit}_{*,y}$ values with the time evolution of the quantities presented in the bottom panel of Fig. 7. When $f^{\rm crit}_{*,y}$ exceeds unity, there is a strong correspondence to a rapid drop in the central gas content of the system. Contrasting the panels within

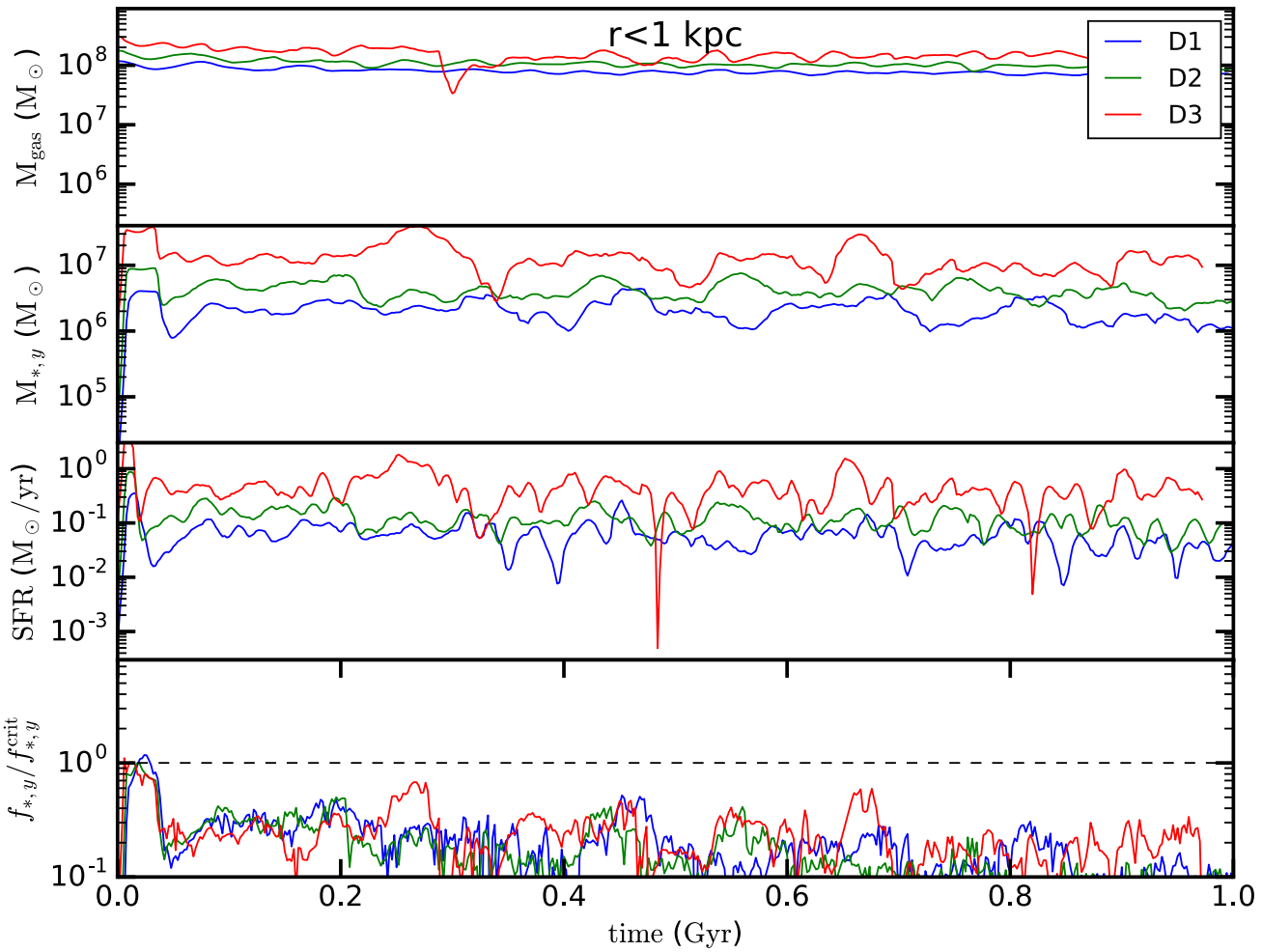

Figure 8. Same as Fig. 7 but for the central 1 kpc. The oscillatory properties that were present for the central 100 pc are not evident for the central 1 kpc. All measured quantities are stable over this larger aperture, in contrast to the 100 pc central region.

Fig. 7 reveals that the $f^{crit}_{*,y}$ values rise much more sharply than the young stellar mass. The driving force behind this feature is that while the mass of young stars is initially responsible for pushing $f^{crit}_{*,y}$ above unity, once this is achieved, the rapid outflow of gas mass from the central region drives up the derived turbulent velocity and drives down the orbital frequency and gas mass. The combination of these three effects results in the very sharp rise of the $f^{crit}_{*,y}$ values. Very large $f^{crit}_{*,y}$ values are not long-lived because (i) the gas fraction drops, (ii) new SF ceases, and soon after, (iii) the mass of young stellar mass decreases (owing to aging).

4.4 Toomre Q and gas velocity dispersions

Further insight into the dynamic behaviour of the central gas reservoir can be obtained from Fig. 9 that shows the Q parameter as a function of time for several disc radii. The Q value is evaluated via $Q = 2c_t\Omega/\pi G\Sigma_g$ using the $\hat{z}$ component of the mass-weighted gas velocity dispersion as a proxy for the turbulent velocity dispersion. Although the horizontal velocity dispersion is formally the quantity entering the Toomre Q parameter derivation, we adopt the vertical, mass-weighted, velocity dispersion because the radial and azimuthal velocity dispersions are more subject to influence by the coherent, non-circular motion of dense clouds in the disc plane. This is a useful substitution assuming that the driven ISM turbulence is at least roughly isotropic. Moreover, the mass- (rather than volume-) weighted velocity dispersion is both more important for the disc dynamics, and less subject to influence from rapidly outflowing material. The Q value hovers around unity consistently with time at large radii, indicating steady-state self-regulation. The smaller radii bins have episodic and strong increases in the Toomre Q value, indicative of local outflows.

The inner regions of the simulated discs experience brief periods of large-gas velocity dispersions coincident with the presence of locally driven outflows. Between these periods, the gas velocity dispersions are of the order of 30–50 km s^{-1}. More specifically, the D1, D2 and D3 discs have median-vertical gas velocity dispersions of in the central 1 kpc of 35.1, 46.3 and 30.7 km s^{-1}, respectively. This is consistent with the prediction that $c_t = f_g\sigma/2$ for $Q = 1$ (our c_t is slightly higher owing to the multicomponent disc and order of unity corrections calculated in Faucher-Giguère et al. 2013). The gas velocity dispersion measured on smaller scales is similar in magnitude (i.e. 30–50 km s^{-1}), but with significantly more variability – particularly around burst episodes.

4.5 Nuclear KS relation

Equilibrium analytic models have been used to explore the low efficiency of SF that is observed in the KS relation (Thompson

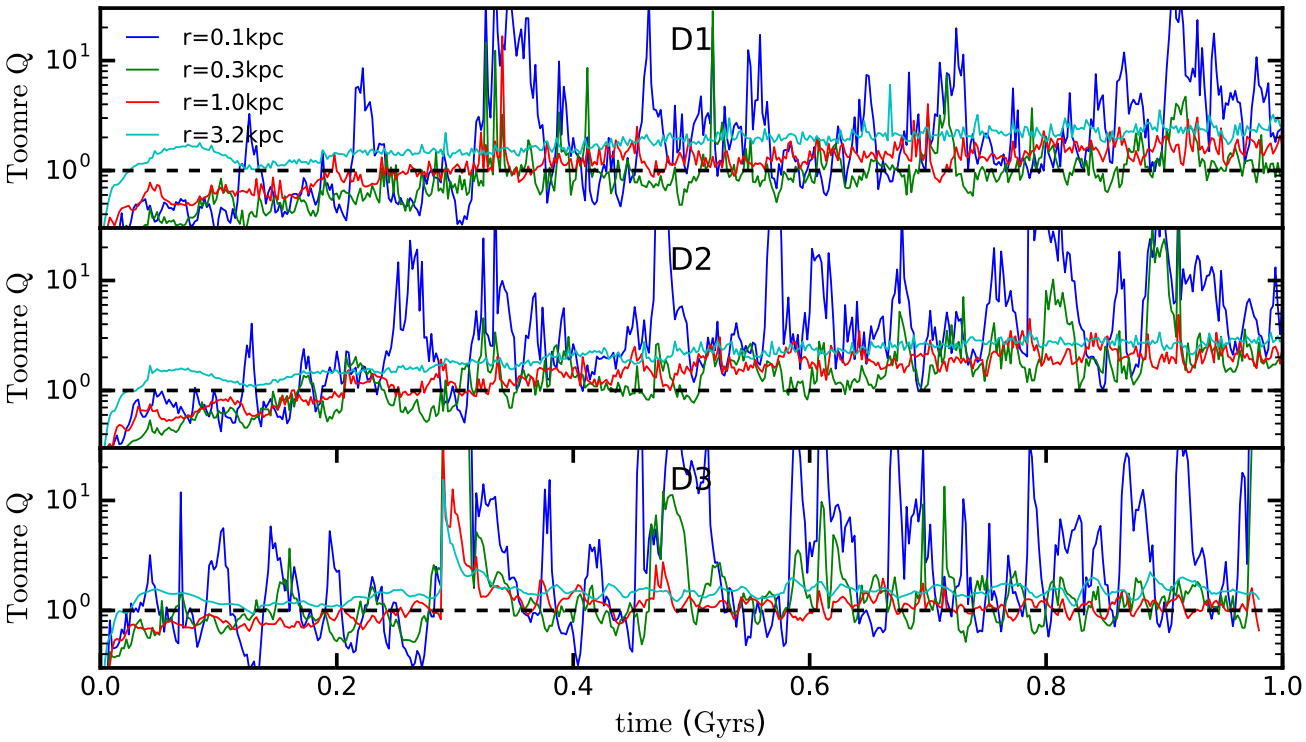

Figure 9. (Left-hand panel) The Toomre Q parameter is shown as a function of time for several radii within each disc. Q approaches unity for all radii. However, while Q hovers around unity consistently with time for the large radii bins, the smaller radii bins have episodic and strong increases in the Toomre Q value. These increases in Q correspond to periods where stellar feedback temporarily dominates the central region's dynamics, and which are indicative of local outflows. (Right-hand panel) The r, ϕ, z velocity dispersion is shown as a function of time for each disc for the central $r = 100$ pc. Steady-state velocity dispersion of $c_t \sim$10–50 km s^{-1} are achieved, with brief excursions to higher velocity dispersion when outflows are being launched.

et al. 2005; Ostriker & Shetty 2011; Faucher-Giguère et al. 2013). Their breakdown may therefore have implications for the KS relation in those regions. In Fig. 10, we consider the $\Sigma_{\rm SFR}$–$\Sigma_{\rm gas}$ KS relation for material within the central $r = 100$ pc (left-hand panel) and 1 kpc (right-hand panel). Fig. 11 shows the $\Sigma_{\rm SFR}$–$\Omega\Sigma_{\rm gas}$ relation – again for material within the central $r = 100$ pc (left-hand panel) and 1 kpc (right-hand panel).[5] SFR surface densities are calculated based on the mass of stars less than 10 Myr old – consistent with the definition of SFR used throughout the rest of this paper.

The KS relation averaged over the central ∼1 kpc is reasonably tight and consistent with the KS relations derived from observations by Bouché et al. (2007) and Faucher-Giguère et al. (2013). The slope of the KS relation predicted by our simulations is roughly n∼2 ($\Sigma_{\rm SFR} \propto \Sigma_{\rm g}^{n}$). This slope is steeper than slopes n∼1–1.5 often derived from observations assuming a constant $X_{\rm CO}$ conversion factor (e.g. Genzel et al. 2010), but is consistent with analytic equilibrium models (Ostriker & Shetty 2011; Faucher-Giguère et al. 2013), and with an interpretation of observations assuming an $X_{\rm CO}$ factor varying continuously with $\Sigma_{\rm g}$ (Ostriker & Shetty 2011; Narayanan et al. 2012). This has been shown already for our adopted ISM/SF/feedback model (Hopkins et al. 2011; Faucher-Giguère & Quataert 2012; Hopkins et al. 2016). The SF efficiency for all three discs hovers around 5 per cent SF efficiency per dynamical time. This is slightly higher than the analytic expectation from equation (7). For the disc turbulent velocities of ∼30–50 km s^{-1}, the analytically predicted SF efficiencies per dynamical time are 2–3.3 per cent.

The smaller aperture KS relations have significantly more scatter than their larger aperture counterparts. The dense cloud of points sitting around $\Sigma_{\rm gas} \sim 10^2$ M$_\odot$ pc^{-2} falls somewhat above the observed KS relation. This is owing to the 100 per cent local SF efficiency per free fall time (at the SF density threshold) that is used in our simulations (e.g. Salim, Federrath & Kewley 2015). Once stars are formed in this cloud, they immediately start acting to clear the nuclear region of gas. Since the SFRs plotted in Figs 10 and 11 are derived from the mass of young stars, we find a cloud of points that extends towards significantly lower gas surface densities. This is a result of measuring the SFR from the mass of young stars that have both formed recently and begun to clear their birth cloud gas, and comparing it against the current gas mass. Re-examination of Fig. 5 confirms how this process takes place in our simulations.

5 DISCUSSION

We have examined the stability of self-regulated SF in galactic nuclei. SF in regions of galaxies with short dynamical times (shorter than the stellar evolution time-scale) cannot reach a truly equilibrium state, but instead undergo 'burst quench' cycles. We presented an analytically motivated model where gas flows into the nuclear region and begins forming stars until enough young stellar mass is present to overwhelm the self-gravity of the gas leading to a localized blowout of the gas.

This is similar to the behaviour of a single GMC (see e.g. Scalo & Struck-Marcell 1986; Fall et al. 2010; Murray et al. 2010) within which the local dynamical time can also become short. The key

[5] For clarity, we take the dynamical time to be $t_{\rm dyn} = 1/\Omega = r/v$. We calculate the dynamical time based on the local potential.

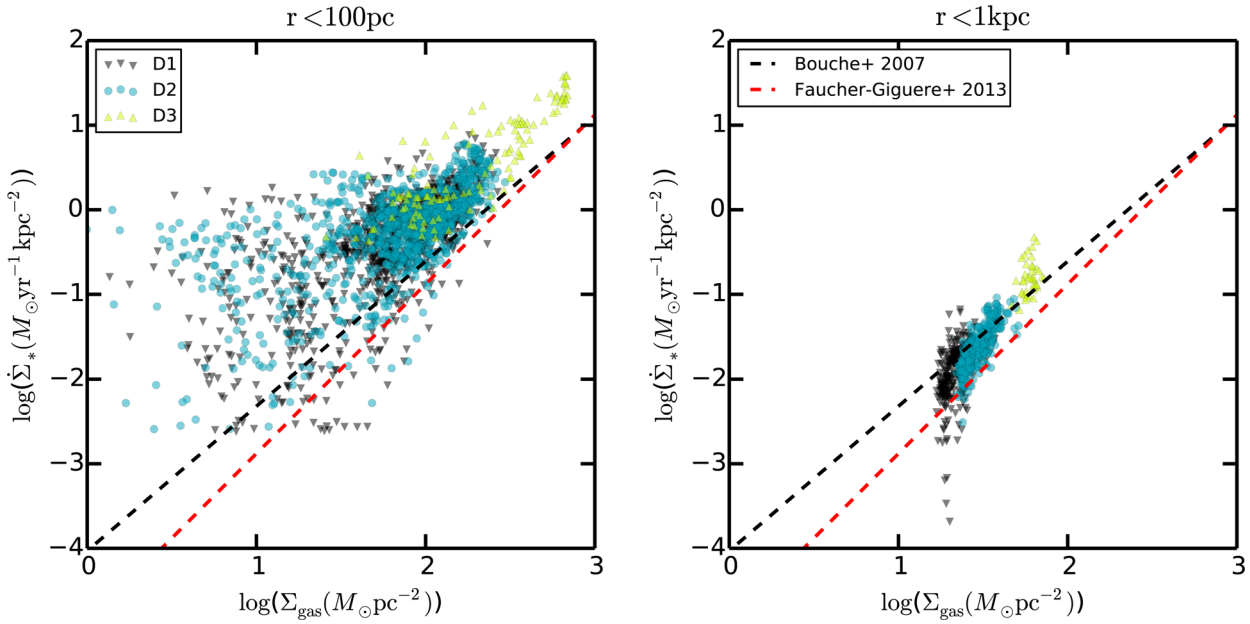

Figure 10. The $\Sigma_{\rm SFR}$–$\Sigma_{\rm gas}$ KS relation is shown for material within the central $r = 100$ pc (left-hand panel) and 1 kpc (right-hand panel). We find significantly increased scatter for the $r = 100$ pc relation compared to larger aperture relation. For comparison, we present the empirically derived KS relations from Faucher-Giguère et al. (2013) and Bouché et al. (2007).

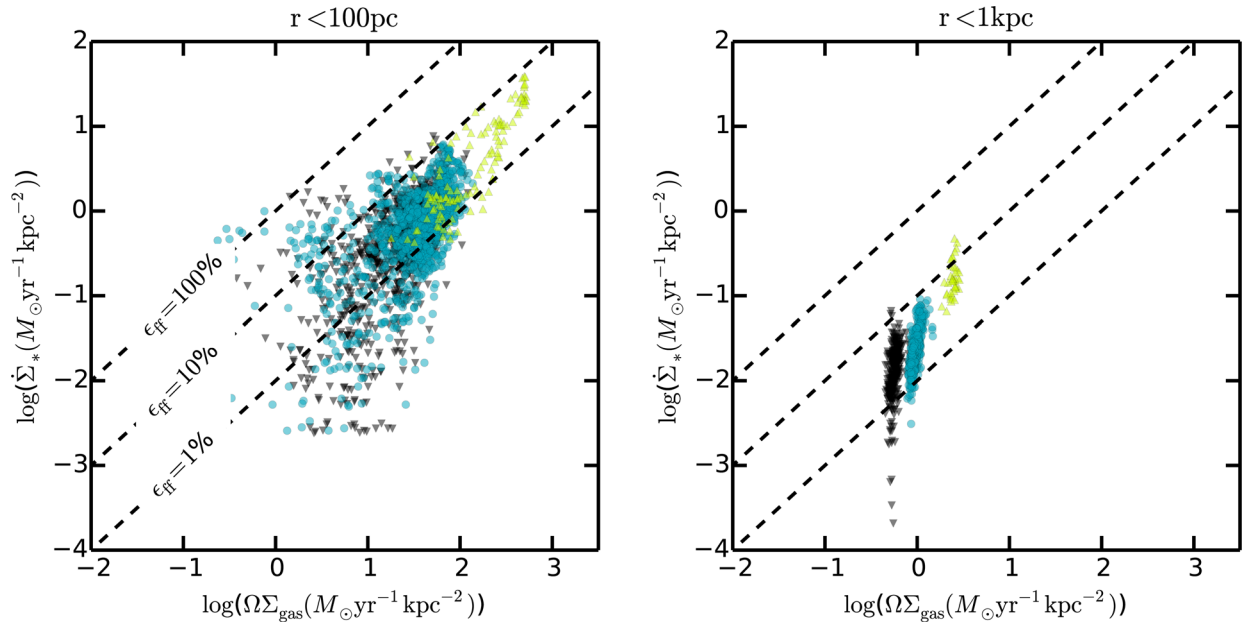

Figure 11. The $\Sigma_{\rm SFR}$–$\Omega\Sigma_{\rm gas}$ relation for material within the central $r = 100$ pc (left-hand panel) and 1 kpc (right-hand panel) is shown. The same legend from Fig. 10 applies. The dashed lines in the plots indicate 1 per cent, 10 per cent and 100 per cent of the gas mass being turned into stellar mass per dynamical time. The SF efficiency in the nucleus has more scatter than that at larger radii.

difference between the nuclear region and a typical GMC is that this behaviour is driven by the collectively short dynamical time of the disc, rather than the local potential of the star-forming gas cloud. SF in the nuclear region can occur in several dense star-forming regions (see e.g. Fig. 5). However, for feedback purposes, massive young stars quickly separate from their birth clouds and the *entire* nuclear region therefore acts as a single short dynamical time region.

Observed nuclear stellar discs show indications of oscillatory SF and feedback cycles. Davies et al. (2007) found that a sample of Seyfert galaxies contained nuclear star clusters with spatial extent $\lesssim 50$ pc. Interestingly, although these nuclear star clusters could be identified to have characteristic ages of ∼10–300 Myr, there was little or no evidence of ongoing SF in these same systems (as inferred through low values for the equivalent widths of Br γ emission). We caution, however, that the modest gas surface densities ($\Sigma_{\rm gas} \lesssim 300\,{\rm M}_\odot$ pc^{-2}) explored in this paper are not directly comparable to the population ($\Sigma_{\rm gas} \gtrsim 1000\,{\rm M}_\odot$ pc^{-2}) studied in Davies et al. (2007). Nuclear star clusters found in nearby late-type (unperturbed) galaxies are better analogues to the

systems discussed in this paper (Walcher et al. 2005; Seth et al. 2006; Georgiev & Böker 2014).

The 'burst-quench' cycle described in this paper may have links to the central molecular zone (CMZ) found in the centre of our own Galaxy (Longmore et al. 2013). Kruijssen et al. (2014) suggested that the SF efficiency in the CMZ could be suppressed through turbulence driven by acoustic instabilities. The low efficiency of SF causes gas to pile up (Krumholz & Kruijssen 2015), which would likely undergo a burst-quench cycle, as described in this paper. Although the one-dimensional models presented in Krumholz, Kruijssen & Crocker (2017) revealed duty cycles that were somewhat shorter than the ∼50-Myr duty cycles quoted in this paper, both Krumholz et al. (2017) and our model predict the ubiquity of 'bursty' SF in the centre of galactic nuclei. In this context, the CMZ of the Milky Way is a natural state in the cycle between gas inflow and gas outflow where gas has returned to the Galactic Centre but not yet become efficiently star-forming.

If there is a link between aging stellar populations and the fuelling of AGN activity, as has been implied from the time offset between nuclear SF and Seyfert activity, then the bursty nature of SF found in our model would have implications for AGN fuelling. Our models included a central supermassive black hole – which is dynamically important for the innermost galactic regions studied in this paper – as well as a stellar mass-loss. However, we elected to not include black hole growth and associated black hole feedback in this study as both processes add significant complicating factors to the interpretation of the results. In the future, we intend to run additional simulations that consider the relationship between nuclear SF and AGN activity (for preliminary results on black hole growth and feedback in simulations focusing on the inner ∼100-pc regions of gas-rich galaxies, see Hopkins et al. 2016).

A particularly interesting application of full galaxy simulations that will include both explicit feedback from stars and from massive black holes in a resolved ISM will be to study the generation and effects of galaxy-scale outflows driven by luminous AGN. Such outflows have now been detected in luminous quasars over a wide range of redshift and in both atomic and molecular gas (e.g. Rupke & Veilleux 2011; Greene, Zakamska & Smith 2012; Cicone et al. 2014; Harrison et al. 2014). These appear energetic enough to potentially strongly affect galaxy scale SF. While idealized analytic and numerical calculations (e.g. Faucher-Giguère & Quataert 2012; Zubovas & King 2012; Costa, Sijacki & Haehnelt 2014; Bourne, Nayakshin & Hobbs 2014) have begun to address the physics of such outflows, fully dynamical simulations of galaxies including both stellar and black hole feedback will likely be needed to robustly predicted how AGN-driven galactic winds are mass-loaded and how they affect the host galaxy.

6 CONCLUSIONS

We have studied the impact of feedback from young stars on the SFRs and gas content of galactic nuclei. We outlined basic analytic arguments that modify existing feedback equilibrium SF models (e.g. Thompson et al. 2005; Ostriker & Shetty 2011; Faucher-Giguère et al. 2013) to apply to short dynamical time regions. We ran and explored numerical simulations that included realistic, time-resolved stellar feedback prescriptions to directly model the evolution of several galaxy models.

Our primary conclusions are as follows:

(i) The nuclear regions ($r \lesssim 100$ pc) of galaxies are characterized by orbital dynamical times of the order of ∼1 Myr. Feedback from young stars evolves over time-scales of tens of Myr (Fig. 1). This time-scale mismatch means that feedback from young stars is not immediately responsive to changes in the gas state, and thus there is no stable stellar feedback regulated equilibrium SFR.

(ii) Instead, gas will continue to form stars until a critical mass of young stars is formed (equation 12), at which point the feedback from young stars leads to an unstable blowout from the nucleus. After the blowout, new gas flows into the nucleus from larger radii (Fig. 4). As a consequence, the gas content, SFR and mass of young stars all oscillate in time when measured over ∼100 pc scales; they are significantly more stable when measured over larger $\gtrsim$ 1-kpc scales (Figs 7 and 8).

(iii) Both short-period (∼10 Myr) variability and long-period (∼100 Myr) burst-quench cycles are observed in the nuclear SF activity. The short-period variability is driven by the formation and destruction of individual GMCs, while the long-period burst-quench cycles are driven by the feedback instability at the core of this paper.

(iv) The simulated KS relation shows very different properties on 100 pc and 1 kpc scales (see Fig. 10). The long dynamical time on large scales means the system can reach equilibrium. This leads to a more stable SFR and gas content with time – hence a tighter KS relation. In the galactic nucleus, by contrast, the KS relation is much more variable and has larger scatter.

In this study, the dynamical effect of the central supermassive black hole was included but AGN feedback was not. In this paper, we have shown that stellar feedback *alone* is capable of driving episodic SF and outflows from galactic nuclei. However, considering both stellar and AGN feedback in concert will be important for understanding the relative importance of different feedback channels on galactic nuclei.

ACKNOWLEDGEMENTS

We thank the referee, Eve Ostriker, for the many thoughtful comments that have strengthened this work. PT acknowledges helpful discussions with Sara Ellison, Nick McConnell and Sarah Wellons. PT is supported through Hubble Fellowship grant #HST-HF2-51384.001-A awarded by the Space Telescope Science Institute, which is operated by the Association of Universities for Research in Astronomy, Inc., for NASA, under contract NAS5-26555. Support for PFH was provided by an Alfred P. Sloan Research Fellowship, NASA ATP Grant NNX14AH35G, NSF Collaborative Research Grant #1411920, and CAREER grant #1455342. CAFG was supported by NSF through grants AST-1412836 and AST-1517491, by NASA through grant NNX15AB22G and by STScI through grant HST-AR-14293.001-A. MV acknowledges support through an MIT RSC award. DK was supported by NSF grant AST-1412153 and Cottrell Scholar Award from the Research Corporation for Science Advancement. EQ was supported in part by NASA ATP grant 12-APT12-0183, a Simons Investigator award from the Simons Foundation, and the David and Lucile Packard Foundation. The simulations reported in this paper were run and processed on the 'Quest' computer cluster at Northwestern University, the Caltech compute cluster 'Zwicky' (NSF MRI award #PHY-0960291), the joint partition of the MIT-Harvard computing cluster 'Odyssey' supported by MKI and FAS, and allocation TG-AST130039 and TG-AST150059 granted by the Extreme Science and Engineering Discovery Environment (XSEDE) supported by the NSF.

REFERENCES

Bigiel F., Leroy A., Walter F., Brinks E., de Blok W. J. G., Madore B., Thornley M. D., 2008, AJ, 136, 2846
Booth C. M., Agertz O., Kravtsov A. V., Gnedin N. Y., 2013, ApJ, 777, L16
Bouché N. et al., 2007, ApJ, 671, 303
Bourne M. A., Nayakshin S., Hobbs A., 2014, MNRAS, 441, 3055
Cicone C. et al., 2014, A&A, 562, A21
Cioffi D. F., McKee C. F., Bertschinger E., 1988, ApJ, 334, 252
Costa T., Sijacki D., Haehnelt M. G., 2014, MNRAS, 444, 2355
Davies R. I., Müller Sáánchez F., Genzel R., Tacconi L. J., Hicks E. K. S., Friedrich S., Sternberg A., 2007, ApJ, 671, 1388
Dolag K., Bartelmann M., Lesch H., 1999, A&A, 348, 351
Fall S. M., Krumholz M. R., Matzner C. D., 2010, ApJ, 710, L142
Faucher-Giguère C.-A., Quataert E., 2012, MNRAS, 425, 605
Faucher-Giguère C.-A., Quataert E., Hopkins P. F., 2013, MNRAS, 433, 1970
Faucher-Giguère C.-A., Hopkins P. F., Kereš D., Keres D., Muratov A. L., Quataert E., Murray N., 2015, MNRAS, 449, 987
Federrath C., Klessen R. S., 2012, ApJ, 761, 156
Gatto A. et al., 2015, MNRAS, 449, 1057
Genzel R. et al., 2010, MNRAS, 407, 2091
Georgiev I. Y., Böker T., 2014, MNRAS, 441, 3570
Greene J. E., Zakamska N. L., Smith P. S., 2012, ApJ, 746, 86
Harrison C. M., Alexander D. M., Mullaney J. R., Swinbank A. M., 2014, MNRAS, 441, 3306
Hennebelle P., Iffrig O., 2014, A&A, 570, A81
Hernquist L., 1990, ApJ, 356, 359
Hopkins P. F., 2015, MNRAS, 450, 53
Hopkins P. F., Quataert E., 2011, MNRAS, 415, 1027
Hopkins P. F., Murray N., Quataert E., Thompson T. A., 2010, MNRAS, 401, L19
Hopkins P. F., Quataert E., Murray N., 2011, MNRAS, 417, 950
Hopkins P. F., Kereš D., Oñorbe J., Faucher-Giguéère C.-A., Quataert E., Murray N., Bullock J. S., 2014, MNRAS, 445, 581
Hopkins P. F., Torrey P., Faucher-Giguere C.-A., Quataert E., Murray N., 2016, MNRAS, 458, 816
Jubelgas M., Springel V., Enßlin T., Pfrommer C., 2008, A&A, 481, 33
Kennicutt R. C., Evans N. J., 2012, ARA&A, 50, 531
Kennicutt R. C. Jr, 1998, ApJ, 498, 541
Kim C.-G., Ostriker E. C., 2015, ApJ, 802, 99
Kim C.-G., Kim W.-T., Ostriker E. C., 2011, ApJ, 743, 25
Kim C.-G., Ostriker E. C., Kim W.-T., 2013, ApJ, 776, 1
Kruijssen J. M. D., Longmore S. N., Elmegreen B. G., Murray N., Bally J., Testi L., Kennicutt R. C., 2014, MNRAS, 440, 3370
Krumholz M. R., Gnedin N. Y., 2011, ApJ, 729, 36
Krumholz M. R., Kruijssen J. M. D., 2015, MNRAS, 453, 739
Krumholz M. R., McKee C. F., 2005, ApJ, 630, 250
Krumholz M. R., Matzner C. D., McKee C. F., 2006, ApJ, 653, 361
Krumholz M. R., Kruijssen J. M. D., Crocker R. M., 2017, MNRAS, 466, 1213
Leitherer C., Ortiz Otálvaro P. A., Bresolin F., Kudritzki R.-P., Lo Faro B., Pauldrach A. W. A., Pettini M., Rix S. A., 2010, ApJS, 189, 309
Leroy A. K., Walter F., Brinks E., Bigiel F., de Blok W. J. G., Madore B., Thornley M. D., 2008, AJ, 136, 2782
Longmore S. N. et al., 2013, MNRAS, 429, 987
Marinacci F., Vogelsberger M., Mocz P., Pakmor R., 2015, MNRAS, 453, 3999
Martizzi D., Faucher-Giguère C.-A., Quataert E., 2015, MNRAS, 450, 504
Mo H. J., Mao S., White S. D. M., 1998, MNRAS, 295, 319
Muratov A. L. et al., 2015, MNRAS, 454, 2691
Murray N., Quataert E., Thompson T. A., 2010, ApJ, 709, 191
Narayanan D., Krumholz M. R., Ostriker E. C., Hernquist L., 2012, MNRAS, 421, 3127
Navarro J. F., Frenk C. S., White S. D. M., 1997, ApJ, 490, 493
Ostriker E. C., Shetty R., 2011, ApJ, 731, 41
Ostriker E. C., McKee C. F., Leroy A. K., 2010, ApJ, 721, 975
Pakmor R., Springel V., 2013, MNRAS, 432, 176
Rupke D. S. N., Veilleux S., 2011, ApJ, 729, L27
Salem M., Bryan G. L., Hummels C., 2014, ApJ, 797, L18
Sales L. V., Marinacci F., Springel V., Petkova M., 2014, MNRAS, 439, 2990
Salim D. M., Federrath C., Kewley L. J., 2015, ApJ, 806, L36
Scalo J. M., Struck-Marcell C., 1986, ApJ, 301, 77
Schmidt M., 1959, ApJ, 129, 243
Seth A. C., Dalcanton J. J., Hodge P. W., Debattista V. P., 2006, AJ, 132, 2539
Shetty R., Ostriker E. C., 2012, ApJ, 754, 2
Silk J., 1997, ApJ, 481, 703
Springel V., 2005, MNRAS, 364, 1105
Springel V., White S. D. M., 1999, MNRAS, 307, 162
Thompson T. A., Quataert E., Murray N., 2005, ApJ, 630, 167
Uhlig M., Pfrommer C., Sharma M., Nath B. B., Enß lin T. A., Springel V., 2012, MNRAS, 423, 2374
Walch S. K., Whitworth A. P., Bisbas T., Wünsch R., Hubber D., 2012, MNRAS, 427, 625
Walcher C. J. et al., 2005, ApJ, 618, 237
Wang P., Abel T., 2009, ApJ, 696, 96
Whitworth A., 1979, MNRAS, 186, 59
Zubovas K., King A., 2012, ApJ, 745, L34
Zuckerman B., Evans N. J., II, 1974, ApJ, 192, L149

This paper has been typeset from a TEX/LATEX file prepared by the author.